

## Enhancement of the Infrared Absorption from Molecular Monolayers with Thin Metal Overlayers

A. Hartstein, J. R. Kirtley and J. C. Tsang

IBM Thomas J. Watson Research Center, Yorktown Heights, New York 10598

(Received 4 April 1980)

The infrared absorption from molecular monolayers is enhanced a factor of 20 by thin metal overlayers or underlayers with use of the attenuated-total-reflection technique. The total enhancement, including contributions from the attenuated-total-reflection geometry, is almost  $10^4$ . This effect is consistent with an electric field enhancement due to collective electron resonances associated with the island nature of the thin metal films.

PACS numbers: 78.30.-j

The vibrational states of molecular monolayers can be studied experimentally with inelastic electron-tunneling spectroscopy,<sup>1</sup> Raman scattering,<sup>2-4</sup> inelastic electron scattering,<sup>5</sup> and infrared absorption.<sup>6,7</sup> In the inelastic electron-tunneling experiments it is necessary for the molecules to be sandwiched between two conducting media. Inelastic electron-scattering experiments must be performed in vacuum and have relatively low energy resolution. Both conventional Raman scattering<sup>6</sup> and conventional infrared absorption<sup>6</sup> from monolayers must be done with high surface-area samples, with consequent difficulties in sample characterization, substrate absorption and fluorescence. Raman scattering from surfaces can become quite strong with thin overlayers<sup>2</sup> or underlayers<sup>3,4</sup> of metal, but so far only Ag and Au with a few molecular monolayers have shown a large enhancement. The attenuated-total-reflectance (ATR) geometry in infrared absorption<sup>7</sup> achieves a large effective surface area without the need for powder samples. In this Letter, we report the first observation of the enhancement of infrared absorption from molecular monolayers due to thin metal overlayers and underlayers in the ATR geometry and show that this technique has application to a number of interesting current problems in surface science.

The samples used in this study consisted of molecular monolayers of organic acids deposited on silicon substrates, either followed by or preceded by the evaporation of a thin metal layer. The sample preparation technique has been described by Hansma and Kirtley.<sup>8</sup> The molecular monolayers used in this study were: 4-nitrobenzoic acid, benzoic acid, and 4-pyridine-COOH. The metal overlayers and underlayers studied were either Ag or Au and were evaporated at room temperature to an average thickness,  $d$

$\leq 60 \text{ \AA}$ , as measured by a quartz crystal thickness monitor. The substrates used were silicon total-internal-reflection plates  $50 \times 20 \times 1 \text{ mm}^3$  cut in the parallelepiped geometry as illustrated in the inset to Fig. 1. The substrates were cleaned with solvents and finally with HF to expose the bare silicon surface. Before the molecular monolayers were deposited, a native oxide about  $15\text{-\AA}$  thick forms on the substrates. Infrared measurements show that this cleaning procedure is sufficient to remove any contamination from the substrates.

The infrared absorption from the molecular

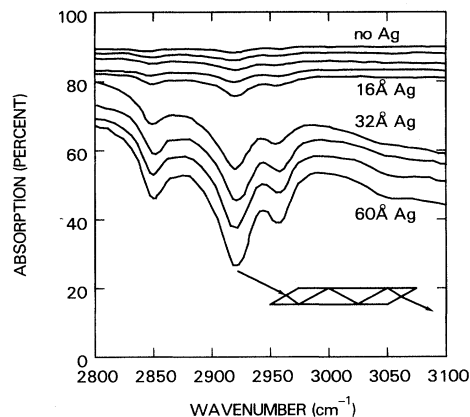


FIG. 1. Absorption of the C-H modes of a monolayer of 4-nitrobenzoic acid. The curves are for increasing thicknesses of a Ag overlayer. The thicknesses are, in order, 0, 2, 4, 8, 16, 32, 40, 50, and  $60 \text{ \AA}$ . The absorption scale is accurate; however, the curves have been offset for clarity. The inset illustrates the path of the infrared radiation through the silicon total-internal-reflection plate. The monolayer sample is deposited on the two sides of the plate.

monolayers was measured using the ATR technique.<sup>7</sup> The path of the infrared radiation through the internal-reflection plate is illustrated in the inset to Fig. 1. The internal angle of incidence was generally chosen to be  $20^\circ$  so that it was close to the critical angle for total internal reflection. For this angle the number of reflections was approximately 140. The angle of incidence was also varied to study the angular dependence of the absorption. The infrared absorption of each of the monolayers was measured both with and without metal overlayers or underlayers.

The ATR technique is only usable over the frequency range for which the substrate is transparent. For silicon this limits the applicable frequency ranges are  $4000\text{ cm}^{-1} \geq \nu \geq 1700\text{ cm}^{-1}$  and  $\nu \leq 420\text{ cm}^{-1}$ . Absorption lines for all of the monolayers were observed at 2950, 2920, 2850, and  $2140\text{ cm}^{-1}$ . The three lines near  $2900\text{ cm}^{-1}$  are identified as C-H stretching modes of the molecule. The line at  $2140\text{ cm}^{-1}$  can be shown to be associated with the Ag itself by looking at samples with Ag overlayers but without the molecular monolayer and may be due to a CN compound at Ag formed from exposure to air.

Figure 1 shows the dependence of the C-H absorption modes of a monolayer of 4-nitrobenzoic acid with increasing thicknesses of a Ag overlayer. The enhancement due to the Ag overlayer is obvious. Figure 2 shows the magnitude of the absorption line at  $2920\text{ cm}^{-1}$  as a function of overlayer thickness as derived from the data shown in Fig. 1. The enhancement is a somewhat complex function of thickness, but it is clear that the effect is not saturating even with  $60\text{ \AA}$  of overlayer coverage. The largest enhancement obtained from the metal overlayer by itself was by a factor of 20. When the metal overlayer gets too thick, the absorption from the metal itself gets too large and no infrared radiation is transmitted through the internal reflection element. This limits the maximum enhancement obtainable in practice.

The question always arises in this type of work as to whether or not a monolayer of material is being observed. Samples made by the same technique have been studied with use of inelastic tunneling spectroscopy<sup>8</sup> and have been shown to be molecular monolayers. In addition our samples with Ag overlayers were measured with Raman scattering and show the same Raman spectra as do the samples used for the tunneling experiments. Therefore, our samples are characterized as monolayers to the same extent as sam-

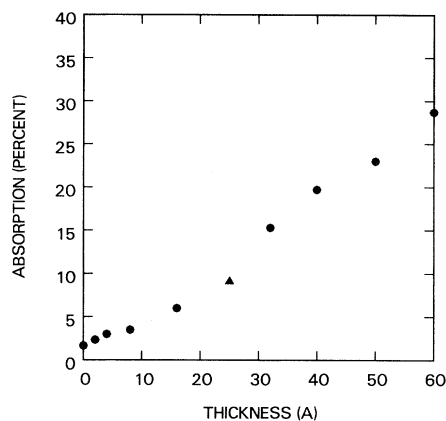


FIG. 2. Dependence of the absorption at  $2920\text{ cm}^{-1}$  on overlayer thickness. The data were obtained by sequentially depositing Ag layers on the same sample. The triangular point was taken with a separately prepared sample.

ples used in other experiments. It is also clear that the sample observed is indeed the molecule deliberately put on the surface, since a Ag layer prepared without the monolayer does not show the presence of C-H stretching modes. This latter point is very important, since the technique used to obtain the data in Fig. 1 was sequentially to deposit Ag and to measure the absorption on the same sample. This procedure could have led to a contamination problem. The form of the dependence of enhancement on thickness shown in Fig. 2 would also not be consistent with a contamination mechanism giving rise to the larger absorptions for larger thicknesses.

Several observations of the nature of the enhancement can be made which bear on the mechanism of enhancement. Overlayers were found to give a larger enhancement than underlayers, although both gave enhancements. Overlayers of Au were measured and found to give the same enhancements as the Ag overlayers. However, the Au was found to be more absorbing, and therefore the range of thicknesses measurable with the Au overlayers was not as large as in the case of Ag. Molecular monolayers of 4-nitrobenzoic acid, benzoic acid, and 4-pyridine-COOH were measured, and the enhancements were found to be the same. These considerations tend to rule out chemical bonding differences as important to the enhancement mechanism. We feel that the most likely mechanism for the enhancement is an electric field enhancement due to collective electron resonances associated with the small islands

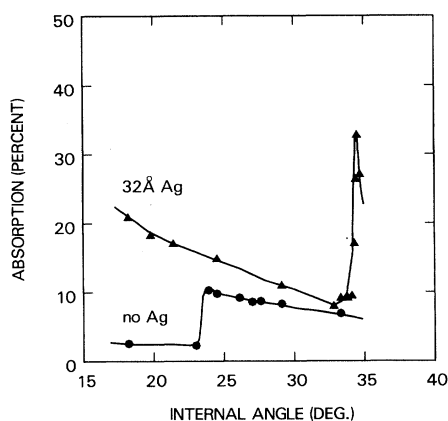


FIG. 3. Dependence of the absorption line at  $2920\text{ cm}^{-1}$  as a function of the internal angle of incidence. Curves for both a monolayer sample and a monolayer sample overcoated with  $32\text{ \AA}$  of Ag are shown. The solid lines are a guide to the eye.

of metal deposited on the samples.<sup>4,9</sup> The magnitude of the enhancement expected from this mechanism at  $3000\text{ cm}^{-1}$  is estimated to be between 6 and 30 for a  $50\text{-\AA}$  overlayer of Ag which is consistent with this experiment. Further evidence for this mechanism comes from two additional observations. The enhancement observed for thick samples ( $\sim 1000\text{ \AA}$ ) is consistent with an enhancement of the top  $35\text{ \AA}$  only. The enhancement disappeared for a  $125\text{-\AA}$  Ag overlayer because the film was nearly continuous (the electrical resistance was  $\sim 300\text{ }\Omega$  for the  $125\text{-\AA}$  film as compared to  $\sim 500\text{ k}\Omega$  for a  $25\text{-\AA}$  film).

The angular dependence of the absorption was measured for samples both with and without a Ag overlayer. The results are shown in Fig. 3. The background trend of lower absorption at higher angles is due to a reduction in the number of internal reflections with increasing angle. It is interesting to note that a discontinuity occurs near the critical angle ( $24^\circ$ ) for total internal reflection between bulk silicon and bulk 4-nitrobenzoic acid for the bare monolayer. However, simple plane-wave multilayer calculations with thin films<sup>7</sup> do not show any large discontinuity near the critical angle. For the sample with a Ag overlayer the discontinuity has shifted, perhaps reflecting an effective medium of 4-nitrobenzoic acid and Ag.

The polarization dependence of the monolayer absorption does not show any striking features. The C-H modes are of comparable intensities in both polarizations perpendicular and parallel to

the surface. This is true for both bare films and films overcoated with Ag. It is expected that when the technique is extended to the other vibrational modes of the monolayers, polarization measurements will yield information about the orientation of the molecules on the surface.

An interesting application of this technique arises from the fact that the C-H vibrational modes of molecular monolayers of 4-pyridine-COOH with Ag overlayers show up only very weakly in both surface enhanced Raman scattering and inelastic electron-tunneling spectroscopy. The observation of strong C-H vibrations in the present experiment indicates that the weakness of the C-H vibrations is specific to the particular measurements involved and does not represent any substantial change in the structure of the molecules at the interface.

In these experiments we have shown for the first time that the infrared absorption due to molecular monolayers can be enhanced by thin metal overlayers and underlayers. The maximum total enhancement observed by this technique over the absorption expected from a single infrared transmission through a monolayer film is close to a factor of  $10^4$ . It is also possible to study the absorption with different metals or without a metal present at all. The absorption intensity is also not strongly dependent on the specific molecule present on the surface. Therefore, this technique would seem to be more flexible in some respects than the complementary techniques of Raman-scattering and inelastic-tunneling spectroscopy which are already being applied to the study of surface monolayers. This technique should complement the others and be very useful as the study of surface adsorbed and absorbed layers progresses.

The authors wish to thank E. Burstein and D. L. Allara for many stimulating discussions on this subject. We also wish to acknowledge the technical assistance of J. A. Kucza and A. M. Torresen.

<sup>1</sup>R. C. Jaklevic and J. Lambe, Phys. Rev. Lett. **17**, 1139 (1966).

<sup>2</sup>J. C. Tsang and J. R. Kirtley, Solid State Commun. **30**, 617 (1979).

<sup>3</sup>D. L. Jeanmaire and R. P. Van Duyne, J. Electroanal. Chem. **84**, 1 (1977).

<sup>4</sup>E. Burstein, C. Y. Chen, and S. Lundquist, in *Light Scattering in Solids*, edited by J. L. Birman, H. Z.

Cummins, and K. K. Rebane (Plenum, New York, 1979), p. 479.

<sup>5</sup>H. Ibach, H. Hopster, and B. Sexton, *Appl. Phys.* **14**, 21 (1977).

<sup>6</sup>A. E. T. Kuiper, J. Medema, and J. J. G. M. Van Bokhoven, *J. Catal.* **29**, 40 (1973).

<sup>7</sup>N. J. Harrick, *Internal Reflection Spectroscopy* (Interscience, New York, 1967).

<sup>8</sup>P. Hansma, *Phys. Rep.* **30C**, 146 (1977); P. K. Hansma and J. R. Kirtley, *Acc. Chem. Res.* **11**, 440 (1978).

<sup>9</sup>T. Yamaguchi, S. Yoshida, and A. Kinbara, *Thin Solid Films* **21**, 173 (1974).

## Resonant Photoemission in Barium and Cerium

A. Zangwill and Paul Soven

*Department of Physics and The Laboratory for Research on the Structure of Matter, University of Pennsylvania, Philadelphia, Pennsylvania 19174*

(Received 9 May 1980)

In this Letter, a theoretical discussion of resonant photoemission in barium and cerium is presented. Calculations are performed using a time-dependent density-functional technique which both is accurate and provides a simple physical interpretation of the resonant phenomena.

PACS numbers: 79.60.Cn

Recent experiments using synchrotron radiation have revealed giant enhancements in the valence-level photoemission from rare-earth metals and compounds which are associated with the large broad maximum observed in photoabsorption above the  $4d$ -ionization threshold.<sup>1,2</sup> For example, the resonant  $4f$  emission is now being used as a "fingerprint" technique to study valence changes in these interesting materials.<sup>3,4</sup> In this work we report the first calculations which exhibit this resonant  $4f$  emission in cerium and illustrate how this effect is common to all the valence levels. In addition, we show that a close connection exists between this and similar behavior observed in the well-studied case of barium photoemission.<sup>5-7</sup> An important aspect of our work is that all the above-mentioned phenomena may be very simply understood within the "local field" framework of our theoretical methods.

Our calculations are based upon a generalization of the Hohenberg-Kohn-Sham density-functional formalism<sup>8</sup> recently introduced in a study of rare gas photoabsorption.<sup>9</sup> The method is essentially a time-dependent local density approximation (TDLDA) in which the external radiation field is replaced by an effective local field,  $\varphi^{\text{SCF}}(\vec{r}, \omega)$ , which self-consistently takes account of the response of the electronic charge density to the external perturbation. Since the total photoabsorption in the vapor and that in the condensed phase are practically identical for both barium and cerium in the photon energy range of interest,<sup>10,11</sup> we have performed all of our calcula-

tions for the case of the free atom.

In the manner of a typical self-consistent field theory, the complex frequency-dependent local field is related to the Fourier components of the time-dependent density disturbance  $\delta n(\vec{r}, t)$ , by the equations

$$\delta n(\vec{r}, \omega) = \int d^3r' \chi_0(\vec{r}, \vec{r}'; \omega) \varphi^{\text{SCF}}(\vec{r}', \omega),$$

$$\varphi^{\text{SCF}}(\vec{r}, \omega) = \varphi^{\text{ext}}(\vec{r}, \omega) + \int d^3r' K(\vec{r}, \vec{r}') \delta n(\vec{r}', \omega).$$

We exactly calculate the retarded density-density response function in the independent-particle approximation,  $\chi_0(\vec{r}, \vec{r}'; \omega)$ ; and the time-independent kernel function is taken to be

$$K(\vec{r}, \vec{r}') = \frac{e^2}{|\vec{r} - \vec{r}'|} + \delta(\vec{r} - \vec{r}') \frac{d}{dn} V_{xc}\{n\}|_{n=n(\vec{r})}.$$

$V_{xc}\{n(\vec{r})\}$  is the exchange-correlation potential commonly employed in a local density approximation (LDA) to density-functional formalism.<sup>12</sup> We wish to emphasize that the structure of our calculation is identical to the random-phase approximation with exchange (RPAE)<sup>5,6</sup>; however, we replace the Hartree-Fock orbitals, eigenvalues, and Coulomb matrix elements by LDA orbitals, eigenvalues, and linearized potentials, respectively. The crucial replacement of the nonlocal Hartree-Fock exchange operator by the local exchange-correlation potential is responsible for the spatially local character of  $\varphi^{\text{SCF}}(\vec{r}, \omega) = \varphi^{\text{ext}}(\vec{r}, \omega) + \varphi^{\text{ind}}(\vec{r}, \omega)$ . In the long-wavelength limit, photoemission cross sections are computed by simply replacing the usual dipole opera-